https://doi.org/10.20965/ijat.2011.p0916

Technical Paper:

Gyroscopic Stabilization of a Self-Balancing Robot Bicycle

Pom Yuan Lam and Tan Kian Sin

Nanyang Polytechnic
180 Ang Mo Kio Avenue 8 Singapore 569830
E-mail: {POM_Yuan_Lam, TAN_Kian_Sin}@nyp.gov.sg
[Received April 13, 2011; accepted October 18, 2011]

This paper reports the design and development of a self-balancing bicycle using off-the-shelf electronics. A self-balancing bicycle is an unstable nonlinear system similar to an inverted pendulum. Experimental results show the robustness and efficiency of the proportional plus derivative controller balancing the bicycle. The system uses a control moment gyroscope as an actuator for balancing.

Keywords: bicycle, Control Moment Gyro (CMG), real-time, control and FPGA

1. Introduction

The bicycle's environmental friendliness and light weight make it a good means of. A robot bicycle is, by nature, an unstable system whose inherent nonlinearity makes it difficult to control. This in turn, brings interesting challenges to the control engineering community. Researchers have been exploring different mechatronic solutions for dynamically balancing and maneuvering robots bicycles.

A self-balancing robot bicycle uses sensors to detect the roll angle of the bicycle and actuators to bring into balance as needed, similar to an inverted pendulum. It is thus an unstable nonlinear system.

A self-balancing robot bicycle can be implemented in several ways. In this report, we introduce these methods, and focus on one of the mechanisms involving a Control Moment Gyro (CMG), – an attitude control device typically used in spacecraft attitude control systems. A CMG consists of a spinning rotor and one or more motorized gimbals that tilt the rotor's angular momentum. As the rotor tilts, changing angular momentum causes gyroscopic precession torque that balances the bicycle.

2. Background

A bicycle is inherently unstable and without apporpriate control, it is uncontrollable and cannot be balanced. There are several different methods for balancing of robot bicycles, such as the use of gyroscopic stabilization by Beznos et al. in 1998 [1], Gallaspy in 1999 [2], moving

Fig. 1. Murata Boy [5], self-balancing bicycle riding robot.

of the Centre Of Gravity (COG) or mass balancing by Lee and Ham in 2002 [3], and steering control by Tanaka and Murakami in 2004 [4]. A very well-known self-balancing robot bicycle, Murata Boy, was developed by Murata in 2005 [5]. Murata Boy (**Fig. 1**) uses a reaction wheel inside the robot as a torque generator, as an actuator to balance the bicycle. The reaction wheel consists of a spinning rotor, whose spin rate is nominally zero. Its spin axis is fixed to the bicycle, and its speed is increased or decreased to generate reaction torque around the spin axis. Reaction wheels are the simplest and least expensive of all momentum-exchange actuators. Its advantages are low cost, simplicity, and the absence of ground reaction. Its disadvantages are that it consumes more energy and cannot produce large amounts of torque.

In another approach proposed by Gallaspy [2], the bicycle can be balanced by controlling the torque exerted on the steering handlebar. Based on the amount of roll, a controller controls the amount of torque applied to the handlebar to balance the bicycle. Advantages of such a system include low mass and low energy consumption. Disadvantages include the ground reaction force it requires and its lack of robustness against large roll disturbance.

Among these methods, the CMG, a gyroscopic stabi-

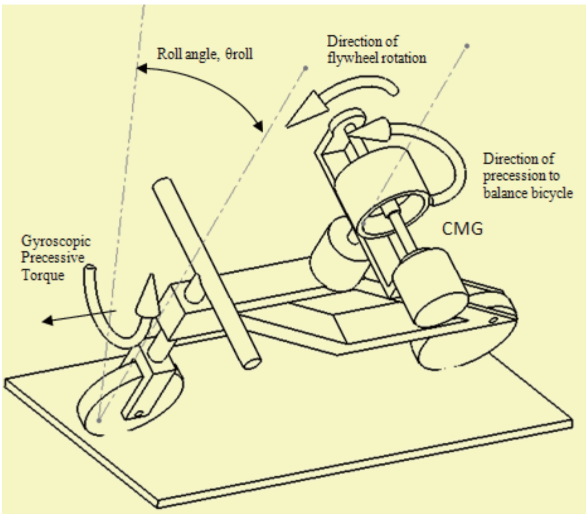

Fig. 2. Balancing of bicycle using gyroscopic precession torque generated by CMG.

lizer is a good choice because its response time is short and the system is stable when the bicycle is stationary. The CMG consists of a spinning rotor with large, constant angular momentum, whose angular momentum vector direction can be changed for a bicycle by rotating the spinning rotor. The spinning rotor, which is on a gimbal, applies torque to the gimbal to produce precessional, gyroscopic reaction torque orthogonal to both the rotor spin and gimbal axes. A CMG amplifies torque because small gimbal torque input produces large control torque to the bicycle. The robot described in this paper uses the CMG as a momentum exchange actuator to balance the bicycle. Advantages of such a system include its being able to produce large amounts of torque and having no ground reaction force. Disadvantages include its greater energy consumption and its greater weight.

3. Dynamic Model of CMG-Controlled Bicycle

The bicycle relies on gyroscopic precession torque to stabilize the bicycle while it is upright. **Fig. 2** shows how precession torque balances the bicycle.

When the bicycle is tilted at angle θ_{roll} as shown in **Fig. 2**, an Inertia Measurement Unit (IMU) sensor detects the roll angle. Roll data is fed to an onboard controller that in turn commands the CMG's gimbal motor to rotate so that gyroscopic precession torque is produced to balance the bicycle upright. The system uses a single gimbal CMG and generated only one axis torque. The direction of output torque change is based on gimbal motion. **Fig. 3** shows the components and vectors of a single gimbal CMG. The system uses gyroscopic torque to balance the bicycle.

The flywheel angular nominal speed is 4480 rpm so ω_{fly} is 469 rad/s.

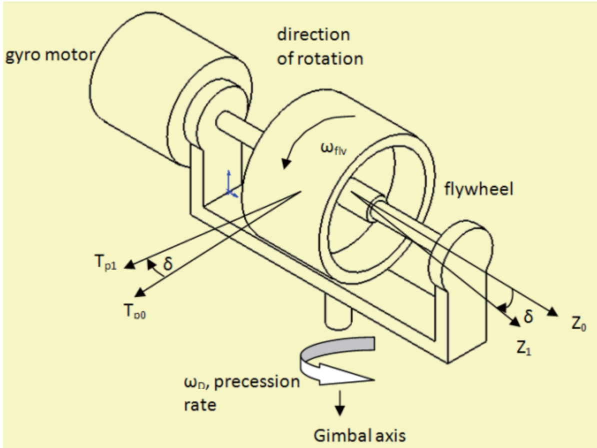

Definition
ω_{fly} is flywheel angular velocity
Z_0 is flywheel angular momentum vector at time t
Z_1 is flywheel angular momentum vector at time (t + dt)
δ is precession angular displacement
Tp_0 is the precessive output torque at time t
Tp_1 is the precessive output torque at time (t + dt)

Material of flywheel	Brass
Mass	2.02kg
Polar moment of inertia, J	8.83E-3 kgm²
Radius of gyration, k	0.066m
Diameter	0.153m
Power	12 W

Fig. 3. Components of a single-axis CMG.

Angular momentum of rotor,

$$\begin{aligned} Z &= J\omega_{\text{fly}} \\ &= 0.00883 \times 469 \\ &= 4.14\ \text{kg} - \text{m}^2/\text{s} \end{aligned}$$

If a rotational precession rate of ω_{D}, is applied to the spinning flywheel around the gimbal axis, precession output torque, T, which is perpendicular to the direction of ω_{fly}, and ω_{D} are generated as shown in **Fig. 3**. The gimbal motor has an angular velocity of 5 rad/s, so the gimbal precession output torque generated is:

$$\begin{aligned} T_{\text{p}} &= J\omega_{\text{D}} \\ &= 4.14 \times 5 \\ &= 20.7\ \text{Nm} \end{aligned}$$

The dynamic model of a bicycle is based on the equilibrium of gravity and centrifugal force. A simplified model for balancing is derived using the Lagrange method and neglecting force generated by the bicycle moving forward and steering. This model is based on the work of Parnichkun [6], which is a simplified dynamics model of the bicycle for balancing control while derived using the Lagrange method and neglecting force generated, as stated, by the bicycle moving forward and steering. With reference to **Fig. 4**, the system, consisting of two rigid body links, has as its first link a bicycle frame having 1 Degree-Of-Freedom (DOF) rotation around the Z axis. The sec-

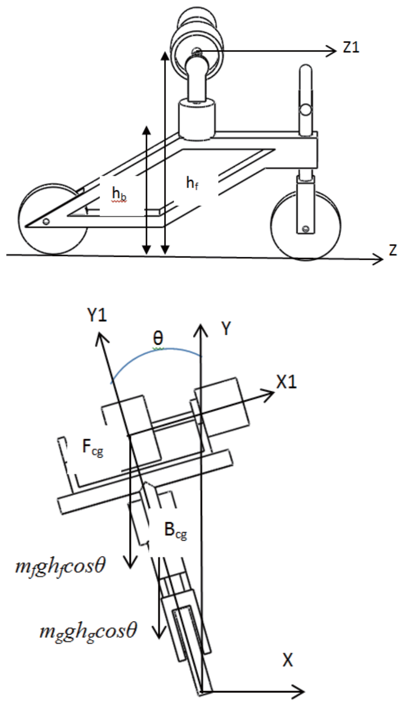

Fig. 4. Reference coordinates of bicycle.

ond link is the flywheel, which is assumed to have constant speed ω. The flywheel COG is fixed relative to the bicycle frame.

When the flywheel rotates at a constant speed around $X1$ axis and we control the angular position of the gimbal axis around the $Y1$ axis, angular momentum on the $Z1$ axis generates a torque, called precession torque, through a gyroscopic effect, and is used to balance the bicycle.

In **Fig. 4**, B_{cg} and F_{cg} denotes bicycle and flywheel COG. The roll angle around the Z axis is defined by θ, and the angular position of the gimbal axis of the flywheel around $Y1$ axis as shown in **Fig. 4**. The angular velocity of the bicycle around the Z axis is defined as $\dot{\theta}$ and the angular velocity of the flywheel around its gimbal axis is defined as $\dot{\delta}$. Since the flywheel COG does not move related to the bicycle COG, absolute velocities of B_{cg} and F_{cg} are:

$$|V_b| = \dot{\theta} h_{\text{B}} \qquad (1)$$

$$|V_f| = \dot{\theta} h_f \qquad (2)$$

where h_b is the height of the bicycle COG in relation to the ground and h_f is the height of the COG of its flywheel counterpart. A Lagrange equation [7] is used to derive the dynamic model of the system:

$$\frac{d}{dt}\left\{\frac{\partial T}{\partial q_i}\right\} - \frac{\partial T}{\partial q_i} + \frac{\partial V}{\partial q_i} = Q_i \qquad (3)$$

where T is total system kinetic energy, V is total system potential, Q_i is external force, and q_i is a generalized coordinate. V and T are determined, represented as follows:

$$V = m_b g h_b \cos\theta + m_f g h_f \cos\theta \qquad (4)$$

$$\begin{aligned} T &= \frac{1}{2}m_b(|v_b|)^2 + \frac{1}{2}m_f(|v_f|)^2 + \frac{1}{2}I_b\dot{\theta}^2 \\ &+ \frac{1}{2}[I_r\dot{\delta}^2 + I_p(\dot{\theta}\sin\delta)^2 + I_r(\dot{\theta}\cos\delta)^2] \\ T &= \frac{1}{2}m_b(\dot{\theta}^2 h_b^2) + \frac{1}{2}m_f(\dot{\theta}^2 h_f^2) + \frac{1}{2}I_b\dot{\theta}^2 \\ &+ \frac{1}{2}[I_r\dot{\delta}^2 + I_p(\dot{\theta}\sin\delta)^2 + I_r(\dot{\theta}\cos\delta)^2] \end{aligned} \qquad (5)$$

where I_p is the flywheel polar moment of inertia and I_r is the flywheel radial moment of inertia, m_b is the mass of the bicycle, and m_f is the mass of the flywheel. I_b is the bicycle moment of inertia.

For $q_i = \theta$, the Lagrange equation becomes

$$\frac{d}{dt}\left\{\frac{\partial T}{\partial \dot{\delta}}\right\} - \frac{\partial T}{\partial \theta} + \frac{\partial V}{\partial \theta} = Q_\theta \qquad (6)$$

Using Eqs. (4)–(6), we have

$$\begin{aligned} &\ddot{\theta}[m_b h_b^2 + m_f h_f^2 + I_b + I_p\sin^2\delta + I_r\cos^2\delta] \\ &+ 2\sin\delta\cos\delta(I_p - I_r)\dot{\theta}\dot{\delta} \\ &- g(m_b h_b + m_f h_f)\sin\theta = I_p\omega\dot{\delta}\cos\delta \end{aligned} \qquad (7)$$

For $q_i = \delta$, the Lagrange equation becomes

$$\frac{d}{dt}\left\{\frac{\partial T}{\partial \dot{\delta}}\right\} - \frac{\partial T}{\partial \delta} + \frac{\partial V}{\partial \delta} = Q_\delta \qquad (8)$$

Using Eqs. (4), (5) and (8) yields the following equation:

$$\begin{aligned} &\ddot{\delta}I_r - \dot{\theta}^2(I_p - I_r)\sin\delta\cos\delta \\ &= T_m - I_p\omega\dot{\theta}\cos\delta - B_m\dot{\delta} \end{aligned} \qquad (9)$$

where B_m is the DC motor viscosity coefficient. The DC motor is coupled to the gimbal of the flywheel via a final 65:1 ratio combining a planetary gear head and belt-drive.

$$T_m = 65K_m i \qquad (10)$$

$$U = L\frac{di}{dt} + R_i + K_e\dot{\delta} \qquad (11)$$

where K_m, K_e are torque and back EMF constants of the motor. R and L are resistance and inductance of the motor. T_m is torque generated by the motor and U is voltage applied to the motor.

4. Bicycle Self-Balancing

Eqs. (7)-(9) model the dynamics of the bicycle. Eqs. (10) to (11) relate the torque generated with the voltage applied to the motor and represent the dynamics of the electrical System.

Combining equations results in:

$$\ddot{\delta}I_r - I_p\omega\dot{\theta} + B_m\dot{\delta} - 65K_m i = 0 \qquad (12)$$

Linearization of the above equations around the equilibrium position ($\theta = \delta = 0$) yields:

$$\ddot{\theta}[m_b h_b^2 + m_f h_f^2 + I_b + I_r] - g(m_b h_b + m_f h_f)\theta - I_p \omega \dot{\delta} = 0 \quad \text{(13)}$$

Define $= \begin{bmatrix} \theta \\ \dot{\theta} \\ \delta \\ \dot{\delta} \end{bmatrix}$, $y = \theta$ and $u = U$. The dynamics model of the system in state-space representation by combining Eqs. (11), (12) and (13) is shown by the following equation:

$$\begin{aligned} \dot{x} &= Ax + Bu \\ y &= Cx + Du \end{aligned} \quad \text{(14)}$$

where

$$A = \begin{bmatrix} 0 & 1 & 0 & 0 \\ \frac{g(m_b h_b + m_f h_f)}{m_b h_b^2 + m_f h_f^2 + I_b + I_r} & 0 & \frac{I_p \omega}{m_b h_b^2 + m_r h_f^2 + I_b + I_r} & 0 \\ 0 & -\frac{I_p \omega}{I_r} & -\frac{B_m}{I_r} & \frac{65 K_m}{I_r} \\ 0 & 0 & -\frac{K_e}{L} & -\frac{R}{L} \end{bmatrix}$$

$$B = \begin{bmatrix} 0 \\ 0 \\ 0 \\ \frac{1}{L} \end{bmatrix}, C = \begin{bmatrix} 1 & 0 & 0 & 0 \end{bmatrix}, \text{ and } D = \begin{bmatrix} 0 \end{bmatrix}. \quad \text{(15)}$$

Table 1 lists the parameters of the self-balancing robot.

Using parameters from **Table 1**, system matrices become:

$$A = \begin{bmatrix} 0 & 1 & 0 & 0 \\ 12.82 & 0 & 1.238 & 0 \\ 0 & -184.6 & -0.133 & 75 \\ 0 & 0 & -22.69 & -5126 \end{bmatrix}$$

$$B = \begin{bmatrix} 0 \\ 0 \\ 0 \\ 840 \end{bmatrix}$$

$$C = \begin{bmatrix} 1 & 0 & 0 & 0 \end{bmatrix}, \text{ and } D = \begin{bmatrix} 0 \end{bmatrix}. \quad \text{(16)}$$

Computing the transfer function from the state variables realization $(\boldsymbol{A}, \boldsymbol{B}, \boldsymbol{C}, \boldsymbol{D})$ yields

$$\frac{\theta(s)}{U(s)} = \frac{780219}{s^4 + 5126.16s^3 + 2602.81s^2 + 1105750s - 30602.6} \quad \text{(17)}$$

Table 1. Caption of table.

Parameters	Value	Unit	Description
m_f	2.02	kg	Mass of flywheel
m_b	8.1	kg	Mass of bicycle
h_f	0.48	m	Flywheel c.g. upright height
h_b	0.42	m	Bicycle c.g. upright height
I_b	1.43	kg·m^2	Bicycle moment of inertia around ground contact line
I_p	0.0088	kg·m^2	Flywheel polar moment of inertia around c.g.
I_r	0.0224	kg·m^2	Flywheel radial moment of inertia around c.g.
ω	469	rad/s	Flywheel angular velocity
L	0.000119	H	Motor Inductance
R	0.61	Ω	Motor Resistance
B_m	0.003	kg·m^2/s	Motor viscosity coefficient
K_m	0.0259	Nm/A	Motor torque constant
K_e	0.0027	V·s	Motor back emf constant
g	9.81	m/s^2	Gravitational acceleration

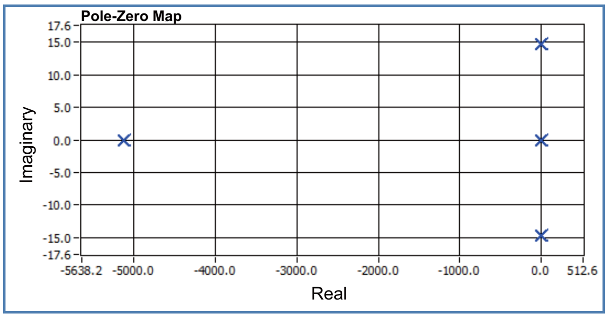

Fig. 5. Pole-zero map of uncompensated-for system.

Computer simulation is used to assess the behavior of the system. The software platform used was the National Instruments Control Design Assistant (CDA).

Pole-zero analysis done showed there are four poles and no zero in the uncompensated-for system. **Fig. 5** shows the pole and zero locations for the uncompensated-for system, which is unstable.

Figure 6 shows a bode plot of the uncompensated-for system. The gain margin was -3.09 and phase margin was -44.04.

A proportional plus derivative controller was implemented in the CDA as shown in **Fig. 7**. Gains were selected by using Ziegler-Nichols rule for tuning and *P*-Gain was selected to be 25 and *D*-gain 0.02.

Figure 8 shows the pole and zero location for the compensated-for system, which is stable.

Figure 9 shows the Bode Plot of the compensated-for system. The gain margin had improved to 6.59 and the phase margin was 86.88. The compensated-for system is stable and pole and zero cancellation can clearly be seen in **Fig. 8**.

Figure 10, shows the effect of increasing *P*-Gain. Overshoot increases with *P*-Gain.

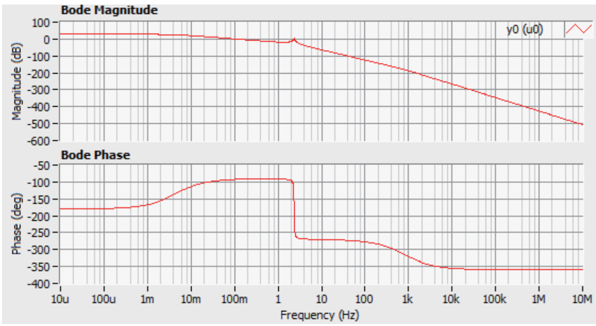

Fig. 6. Bode plot of uncompensated-for system.

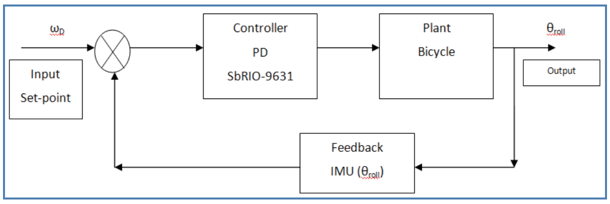

Fig. 7. Control block diagram.

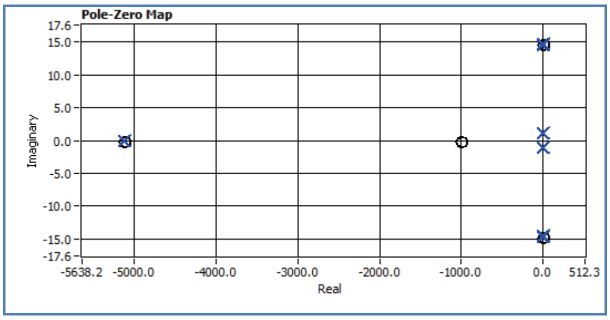

Fig. 8. Pole-zero map of compensated-for system.

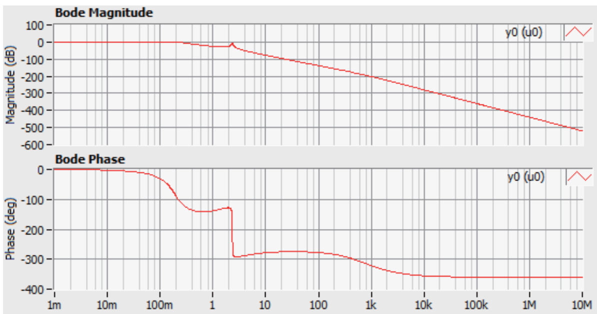

Fig. 9. Bode plot of the compensated-for system.

A PID controller was used instead of a PD controller. **Fig. 11** shows the pole-zero map with the PID controller. The phase margin decreased dramatically and the system becomes unstable and unable to balance the bicycle.

5. Real-Time Experiments

Figure 12 shows the complete mechanical system which consists of an off-the-shelf miniature bicycle and

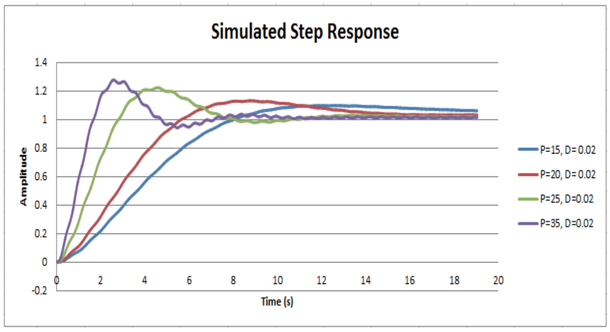

Fig. 10. Simulated step response of the compensated-for system.

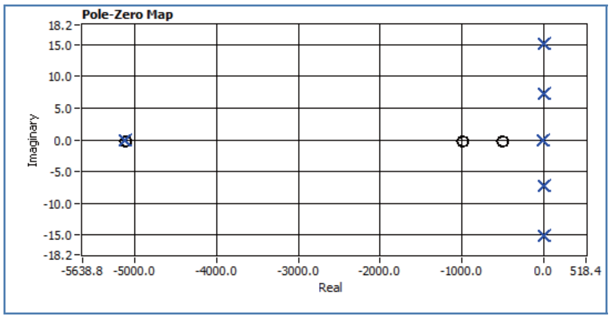

Fig. 11. Pole-zero map of system with PID controller.

a customized CMG on the bicycle frame.

The embedded controller is a single-board reconfigurable IO (SbRIO, National Instruments) consisting of a real-time processor, a reconfigurable Field-Programmable Gate Array (FPGA), and 110 bidirectional digital I/O lines along with RS232, Ethernet, and analog I/O on a single board. All I/O is connected directly to the FPGA, providing low-level customization of timing and I/O signal processing.

An xsens MTi IMU is used to detect the roll angle of the bicycle. The MTi is a miniature, gyro-enhanced Attitude and Heading Reference System (AHRS). Its internal low-power signal processor provides drift-free 3D orientation and calibrated 3D acceleration, a 3D rate of turn, and 3D earth-magnetic field data. The MTi is an excellent measurement unit (IMU) for stabilization and control of cameras, robots, vehicles, and other stand-alone equipment. The MTi IMU communicates with the SbRIO via RS232 serial communication at a baud-rate of 115200 bps.

The CMG's flywheel is driven by a Maxon DC motor and is powered by constant dc voltage. The CMG gimbal is driven by a Maxon brushless motor. Encoder signals are fed back to the FPGA of the SbRIO to be processed as angular positioning data.

To have a robust sensing system, differential encoder signals are fed back to the FPGA for processing and normally require additional circuits such as an inverter and an OR gate as show in **Fig. 13**.

With LabVIEW Embedded for FPGA, this can be easily implemented within the FPGA without the need for physical additional circuits.

A PC is connected via the Ethernet to the SbRIO for

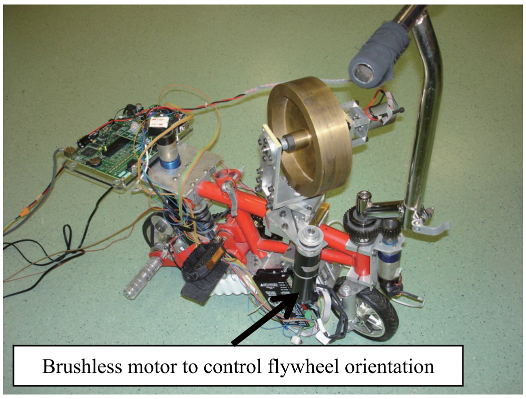

Fig. 12. Bicycle with CMG.

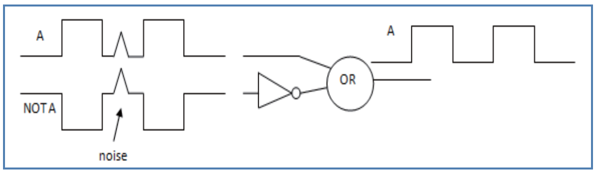

Fig. 13. Circuit to eliminate distortion by complementary encoder signals (differential).

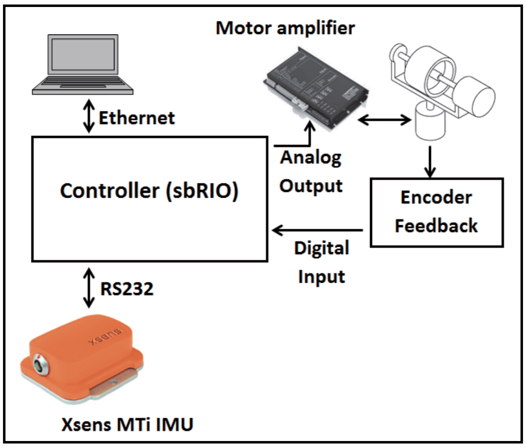

Fig. 14. Electronic system subcomponents.

software development and tuning gains. **Fig. 14** summarizes the electronic system.

Critical encoder positioning data are sampled by the FPGA. Analog output voltage for controlling the gimbal motor is sent from the FPGA. The closed-loop PID controller resides in the Freescale Power PC real-time processor. With LabVIEW Real-Time, PID gains were tune on the fly via an Ethernet connection which greatly reduced gain tuning as opposed to conventional programming.

Embedded controllers are usually programmed with the control algorithm with gains set constant at programming. If gains must be changed, which is done in most cases, the entire embedded controller with new gains must be reprogrammed, which is very inefficient and time-consuming.

In our approach, enable with NI SbRIO and LabVIEW real-time, we are able to tune gains at run time, and, at the same time, view response graphs from the system. Critical parameters such as overshoot and system response can be easily analyzed at run time.

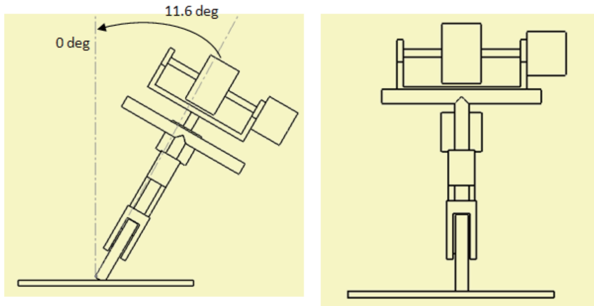

Fig. 15. Experiment setup for step response.

Table 2. Results of critical parameters.

$P = 37$, $D = 0.04$	T_{peak} (s)	1.132
	%OS	6.7
	T_{rise} (s)	0.29
$P = 42$, $D = 0.04$	T_{peak} (s)	1.086
	%OS	4
	T_{rise} (s)	0.178
$P = 47$, $D = 0.04$	T_{peak} (s)	0.726
	%OS	12.7
	T_{rise} (s)	0.146

Ziegler-Nichols rules for tuning PD gains were used to tune gains of the controller [8]. Only proportional control action is used at first to attempt to balance the bicycle. K_p is increased from 0 to critical value K_{cr} while the system exhibits sustained oscillation, or in other words, the bicycle is just about to be balanced around the vertical position. The period of oscillation P_{cr} is measured from the response. Selected K_p will be $0.6 \times K_{cr}$ and selected T_d is $0.125 \times P_{cr}$. Gains were further fine-tuned to ensure that the system can withstand significant roll disturbance. The actual P-Gain used differs from those found in simulation and a P-Gain of 42 is used. **Fig. 15** shows the test setup.

The bicycle is initially tilted at an angle of 11.6 deg and the controller commands the bicycle to take an upright position. Roll data is captured for different PD values.

Figures 16 to **18** shows the result for varying the Proportional gain from 37 to 47 while keeping Derivative gain constant at 0.04.

The result for peak time (T_{peak}), percent overshoot (%OS) and rise time (T_{rise}) is shown in **Table 2**.

P-gain is kept constant while D-gain is varied. The various roll response from varying D-gain are shown in **Figs. 19** to **22**.

The final gains to be used for balancing the bicycle have a P-gain of 47 and D-gain of 0.04. This is selection is a tradeoff between performance and stability. As can be seen from **Fig. 18**, these gain sets produce a relativity fast response and acceptable steady state oscillation of within ± 1.5 deg.

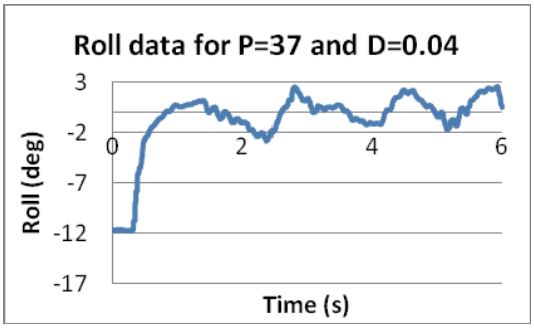

Fig. 16. Roll data for $P = 37$ and $D = 0.04$.

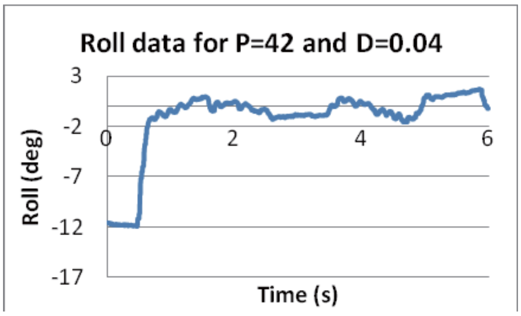

Fig. 17. Roll data for $P = 42$ and $D = 0.04$.

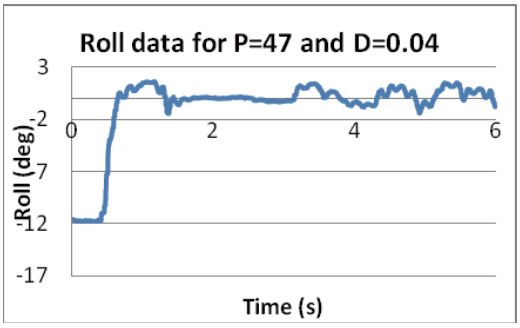

Fig. 18. Roll data for $P = 47$ and $D = 0.04$.

6. Conclusions

This paper has proposed the use of a Control Moment Gyro (CMG) and a PD controller to balance a bicycle. The CMG was used as a momentum exchange actuator to balance the bicycle. The CMG is an effective torque amplification device and has a short response time.

A state space model of the bicycle with the CMG and a closed-loop controller was created in the control design assistant developed by National Instruments. Simulations were used to determine the performance of the controller and to find initial gains to be used in a real-time system for deployment. Simulation exercises showed that a PD controller is adequate for balancing the bicycle. A PID decreases the phase margin dramatically and the system becomes unstable and unable to balance the bicycle.

The real-time controller was implemented on a SbRIO and programmed in LabVIEW. This approach dramatically shortened development time for the PD controller, and was made possible thanks to easy graphical Lab-

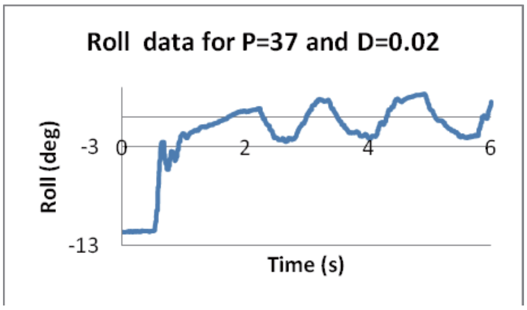

Fig. 19. Roll data for $P = 37$ and $D = 0.02$.

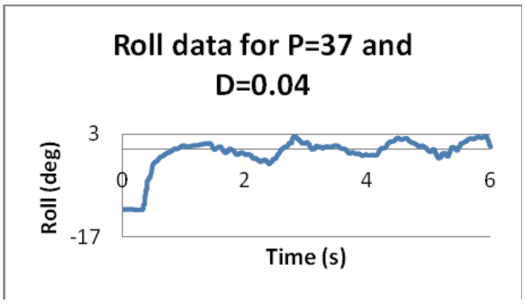

Fig. 20. Roll data for $P = 37$ and $D = 0.04$.

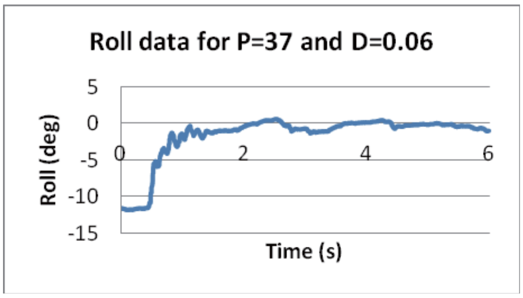

Fig. 21. Roll data for $P = 37$ and $D = 0.04$.

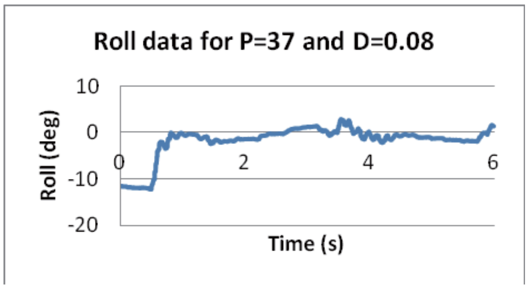

Fig. 22. Roll data for $P = 37$ and $D = 0.04$.

Table 3. Peak-to-peak oscillation.

	Peak-to-peak oscillations (deg)
$P = 37,\ D = 0.02$	4
$P = 37,\ D = 0.04$	4
$P = 37,\ D = 0.06$	2
$P = 37,\ D = 0.08$	5

VIEW programming, enabling data to be easily viewed and manipulated at run-time. With the possibilities of FPGA programming within LabVIEW, this has further enhanced the capability of LabVIEW for embedded applications. Filters can, for example, be easily added at no extra hardware cost.

References:

[1] A V. Beznos, A. M. Formalsky, E. V. Gurfinkel, D. N. Jicharev, A. V. Lensky, K. V. Savitsky et al., "Control of autonomous motion of two-wheel bicycle with gyroscopic stabilization," In:Proc. of the IEEE int. conf. on robotics and automation, p. 2670-5, 1998.

[2] J. M. Gallaspy, "Gyroscopic stabilization of an unmanned bicycle," M.S. Thesis, Auburn University, 1999.

[3] S. Lee, W. Ham, "Self-stabilizing strategy in tracking control of unmanned electric bicycle with mass balance," IEEE int. conf. on intelligent robots and systems, p. 2200-5, 2002.

[4] Y. Tanaka, T. Murakami, "Self sustaining bicycle robot with steering controller," In: Proc. of int. workshop on advanced motion control, 2004, p. 193-7.

[5] The Murata Boy Website. [Online].
Available from http://www.murataboy.com/en/

[6] T. T. BUI and M. Parnichkun, "Balancing of Bicyrobo by particle swarm optimisation based structure-specified mixed H2/H∞ control," Int. J. of Advanced Robotic Systems, 5(4), 395-402, 2008.

[7] S. Wolfram, "Analytical robotics and mechatronics," New York: McGraw-Hill, 1995.

[8] K. Ogata, "Modern Control Engineering," Prentice Hall, 1998.

Name:
Pom Yuan Lam

Affiliation:
Lecturer, Nanyang Polytechnic

Address:
180 Ang Mo Kio Avenue 8 Singapore 569830

Brief Biographical History:

2000- R&D Engineer at Olympus Technologies Sinapore Pte Ltd
2003- R&D Carriage Servo Engineer (Business Printing) at Hewlett Packard Singapore Pte Ltd
2006- Lecturer at Nanyang Polytechnic, Singapore

Main Works:

• Design and development of legged robots, control of unstable system

Name:
Tan Kian Sin

Affiliation:
Nanyang Polytechnic

Address:
180 Ang Mo Kio Avenue 8 Singapore 569830